bioRxiv preprint doi: https://doi.org/10.1101/568147; this version posted March 5, 2019. The copyright holder for this preprint (which was not certified by peer review) is the author/funder. All rights reserved. No reuse allowed without permission.

Human liver organoids; a patient-derived primary model for HBV Infection and Related Hepatocellular Carcinoma

Authors: Elisa De Crignis[1], Fabrizia Carofiglio[1], Panagiotis Moulos[2], Monique M.A. Verstegen[3], Shahla Romal[1], Mir Mubashir Khalid[1], Farzin Pourfarzad[4], Christina Koutsothanassis[5], Helmuth Gehart[6], Tsung Wai Kan[1], Robert-Jan Palstra[1], Charles Boucher[7], Jan M.N. IJzermans[3], Meritxell Huch[8], Sylvia F. Boj[4], Robert Vries[4], Hans Clevers[6], Luc van der Laan[3], Pantelis Hatzis[2], Tokameh Mahmoudi[1*]

Affiliations:

[1] Department of Biochemistry, Erasmus University Medical Center, Ee634 PO Box 2040 3000CA Rotterdam, the Netherlands

[2] Biomedical Sciences Research Center 'Alexander Fleming', 16672 Vari, Greece

[3] Department of Surgery, Erasmus University Medical Center, PO Box 2040 3000CA Rotterdam, the Netherlands

[4] Foundation Hubrecht Organoid Technology (HUB), 3584 CT Utrecht, the Netherlands

[5] HybridStat Predictive Analytics, 34 Panos Street, 16672 Vari, Greece

[6] Hubrecht Institute-KNAW, University Medical Centre Utrecht, CancerGenomics.nl, Uppsalalaan 8, 3584 CM Utrecht, the Netherlands

[7] Department of Viroscience, Erasmus Medical Centre, Rotterdam, the Netherlands

[8] Wellcome Trust/Cancer Research UK University of Cambridge. Tennis court Road, CB2 1QN, Cambridge United Kingdom

[*] Correspondence to: Tokameh Mahmoudi: t.mahmoudi@erasmusmc.nl, Phone N: +31 (0)107043331, Fax N: +31(0)10704747

bioRxiv preprint doi: https://doi.org/10.1101/568147; this version posted March 5, 2019. The copyright holder for this preprint (which was not certified by peer review) is the author/funder. All rights reserved. No reuse allowed without permission.

Abstract The molecular events that drive Hepatitis B virus (HBV)-mediated transformation and tumorigenesis have remained largely unclear, due to the absence of a relevant primary model system. Here we interrogate the potential of human liver organoids as a platform for modeling HBV infection and related tumorigenesis. We show that organoids derived from HBV-infected patients display an aberrant early cancer gene signature, which clusters with the HCC cohort on the TCGA LIHC dataset and away from healthy liver tissue. Furthermore, we demonstrate HBV infection in healthy donor liver organoids after challenge with recombinant virus or HBV infected patient serum. Ex vivo infected liver organoids produced cccDNA, expressed intracellular HBV RNA and proteins, and produced infectious HBV. HBV replication supported by ex vivo infected liver organoids was blocked by treatment with Tenofovir, highlighting the potential of this model system as a primary differentiated hepatocyte platform for HBV drug screening. Interestingly, transgenic organoids exogenously over expressing the HBV receptor NTCP by lentiviral transduction are not more susceptible to HBV, suggesting the necessity for additional host factors for efficient infection. Finally, we generated transgenic organoids harboring integrated HBV, representing a long-term culture system also suitable for viral production and the study of HBV transcription.

bioRxiv preprint doi: https://doi.org/10.1101/568147; this version posted March 5, 2019. The copyright holder for this preprint (which was not certified by peer review) is the author/funder. All rights reserved. No reuse allowed without permission.

Persistent HBV infection is the leading cause of chronic liver cirrhosis and hepatocellular carcinoma (HCC) world-wide[1,2]. A combination of viral and host factors determines whether an individual infected with HBV will be able to clear the infection or will become a chronic carrier. Characterized by its high-host-species and organ-specificity, HBV infection and replication is thought to orchestrate an interplay between the immune system and viral-specific factors that eventually lead to the onset of HCC. Insights into the molecular mechanisms underlying HBV-induced HCC have largely been provided by epidemiological studies[3,4] and genome wide analysis of viral and host characteristics[5-10], as well as by studies performed in in vitro settings using hepatoma cell lines[11,12].

However, a major deficiency attributed to the strict viral host and cell type tropism is the limited availability of relevant animal or in vitro model systems. chimpanzees remain the only animal model that supports the full HBV replication cycle, while available hepatoma cell line models are unsuitable for delineating the molecular steps towards tumorigenesis as they differ substantially from primary cells in their already tumor-derived gene expression profiles. Primary hepatocytes present the gold standard model system for HBV research in vitro. However they are difficult to obtain and rapidly lose their phenotype when cultured. More recently reports describe induced pluripotent stem cell (iPSC)-derived hepatocytes, which are susceptible to HBV infection and support replication, providing a useful tool for studying host-virus determinants of replication[13-15]. However, limitations in the half-life and spread of this replicating culture system together with its long differentiation processes is limiting. As a consequence of deficiencies in available model systems, despite its fascinating biology, many questions regarding the life cycle of HBV, its mechanisms of persistence, and the HBV-induced molecular events underlying tumorigenesis remain largely unexplored in primary settings, and key viral and host players involved remain unknown.

The dependence of liver hepatocytes on spatial and matrix-derived signals[16-18] and their limited half-life in traditional cell culture has limited the development of primary HBV replication platforms suitable for drug screening. Recently, we have established a novel primary liver culture system based on isolation and expansion of primary cells that allows for the long-term expansion of liver cells as so called organoids[19,20]. Liver organoids retain the ability to differentiate when cultured in media containing specific growth factors, and display the characteristics of differentiated hepatocytes[20], thereby representing a primary in vitro cell culture platform for the molecular and mechanistic examination of liver disease and tumorigenesis[21].

bioRxiv preprint doi: https://doi.org/10.1101/568147; this version posted March 5, 2019. The copyright holder for this preprint (which was not certified by peer review) is the author/funder. All rights reserved. No reuse allowed without permission.

Results

HBV infected patient-derived liver organoids display an early cancer gene expression signature

We exploited the procedure for isolation and establishment of healthy liver organoid cultures[20] to establish the first primary culture system from HBV infected patients undergoing liver transplantation (Fig. 1a). In the latter, the explant is characterized by HBV-induced chronically cirrhotic liver tissue. We established organoid cultures starting from cirrhotic tissue obtained from eleven explanted HBV infected livers (Table S1, Fig. 1a and b) and a biopsy obtained from an HBV-infected but cleared donor whose liver was functional and eligible for transplantation (Table S1, iP-B). We generated and expanded organoid cultures from fresh and frozen explant tissue from all donors with similar efficiency.

Non-tumor, HBV-infected, patient-derived (iP) organoids were expanded in culture (EM) and displayed proliferation rates (Fig. 1b and data not shown) and expression of progenitor markers LGR5, KRT7, HNF4α, and Sox9 (Fig. 1c) comparable to that of healthy donor (hD) organoids. When grown in differentiation medium (DM), in which proliferation signals are removed and the progenitor fate is inhibited, liver organoid cultures acquire hepatocyte fate and differentiate into functional hepatocytes in vitro[20]. In DM, iP liver organoid cultures, as we have shown in hD liver organoid cultures[20] showed increased expression of hepatocyte-specific genes Albumin and Cytochrome C3A4 , and the recently identified cellular receptor for HBV hepatocyte entry Sodium taurocholate co-transporting polypeptide (NTCP), concomitant with decreased expression of the stem cell-specific gene LGR5 (Fig. 1d and Supplementary Fig. 1). None of the iP organoids showed signs of HBV production at the RNA, DNA or protein level (data not shown), suggesting that liver progenitors do not support HBV replication. At the phenotypic level, while EM organoids grew larger in size and were translucent, differentiated iP organoids showed hepatocyte morphology and a thickening of the outer cell layer, comparable to hD organoids (Fig. 1e and Supplementary Fig. 1) and produced comparable levels of albumin as detected by immunofluorescence staining (Fig. 1e and Supplementary Fig. 1). Thus, non-tumor HBV iP and hD organoids display comparable phenotypes and capacity for differentiation.

To further characterize iP organoids, we performed mRNA sequencing of the organoid lines derived from HBV iP and compared their gene expression profile to that of hD organoids. We performed hierarchical clustering of protein-coding differentially expressed genes obtained from the comparison between organoids of five hD organoid lines with five iPs (iPs -BC and -BCC1-4) (Fig 1f). The iP

bioRxiv preprint doi: https://doi.org/10.1101/568147; this version posted March 5, 2019. The copyright holder for this preprint (which was not certified by peer review) is the author/funder. All rights reserved. No reuse allowed without permission.

organoid lines were seeded from five HBV mono-infected patients with cirrhotic liver, four of which presented with small tumors at the time of explant) (Fig 1F, Table S1). This comparison resulted in identification of an iP-characteristic "gene signature" (Fig. 1f and Supplementary Table S2).

The early detection of HBV-related HCC is a challenge that remains critical to direct optimal clinical management of the disease. The presence of diagnostic biomarkers for early events in liver cell tumorigenesis would therefore be invaluable to early detection. In order to identify potential early biomarker genes for HBV-induced HCC, we ranked the differentially expressed genes according to the relative distance of their expression in hD versus HBV-iP derived organoids and identified a group of 33 putative early biomarker genes (Fig. 2a). Among these, CCNA1, STMN2, , which we found were upregulated in the non-tumor patient-derived organoids, were previously identified to be upregulated in HCC[22-25]. Conversely, WNK2, RUSC2, CYP3A4 and RGN, among the significantly downregulated genes in the non-tumor iP organoids have been described as tumor suppressors downregulated in HCC[22,26-28].

GO-term and KEGG-pathway analysis revealed that the "early signature" genes were enriched in metabolic pathway-associated genes (Table S3). Importantly, this signature, when applied to all iP and hD samples, perfectly groups the healthy (grey) against the HBV-infected samples (black) (Fig. 2b). In addition, the early signature groups the HBV-infected iP organoids (purple) and the HBV/HDV co-infected iP organoids closely together (light blue). The signature also separates the non-infected samples (green) and groups the iP organoids derived from patients who had HCC (red) as well as those derived from patients with acute liver failure (dark blue). Interestingly, iP-B and iP-BC, which are organoids derived from HBV-infected patients not displaying HCC, cluster together and closely to the larger group of iP organoids derived from patients with HCC (iP-BCC1-4). Notably, iP-B, derived from a liver clear of HBV infection at the time of donation, is the less similar in the group, yet still clustered with the HCC patients but away from the acute liver failure patient organoids, as indicated by the dendrogram branch to which iP-B belongs (Fig. 2b). In agreement, multidimensional scaling analysis of all iP and hD samples indicates that all hD organoids are clearly separated from the rest and tightly grouped together, while the iP organoids form separate groups. We have therefore identified a specific gene signature/group which discriminates the hD and iP organoids among more complex classifications (Fig. 2c). Finally, the signature separates the TCGA LIHC samples from non-HCC tissue, when mapped onto the relevant TCGA gene expression data (Fig. 2d). Our data demonstrates that HBV iP-derived liver organoids are a primary cell culture model that resembles its diseased tissue

bioRxiv preprint doi: https://doi.org/10.1101/568147; this version posted March 5, 2019. The copyright holder for this preprint (which was not certified by peer review) is the author/funder. All rights reserved. No reuse allowed without permission.

of origin. Importantly, the model identified a novel early liver cancer gene signature in non-tumor HBV-infected patient-derived liver organoids, despite the absence of phenotypic signs of aberrant growth.

Human liver organoids allow modelling of HBV infection in vitro

To establish a defined in vitro primary model system for HBV infection and tumorigenesis, we infected hD liver organoids with HBV. Organoids were grown in either EM or DM for 7 days prior to infection with HBV or heat inactivated HBV (HI) (Fig. 3a-b). HBV infection and replication were determined by quantifying the levels of HBV DNA in the supernatant and examining the presence of HBV RNA and HBV specific proteins in infected cells. HBV DNA was detected in organoid culture supernatants from four days post infection indicating the presence of viral replication (Fig. 3b). NTCP, the cellular receptor for HBV hepatocyte entry, was strongly upregulated during differentiation while detectable at low levels in EM organoids (Supplementary Fig. 2). Accordingly, differentiated organoids maintained in DM were more efficiently infected and produced higher viral titers (Fig. 3b-c). The RNA intermediates necessary for protein production and viral replication (HBV pol and Hbx) were present in infected organoids and detected by RT-PCR analysis (Fig. 3c and 3e). Furthermore, immunostaining using antibodies recognizing the HBV core (HBcAg) confirmed the presence of foci of HBV replication in the cultures (Fig. 3d). Viral DNA, RNA and HBcAg were detected both in EM and DM (differentiated) organoid cultures. However, consistent with the higher levels of NTCP expression, levels of HBV replication were higher in differentiated organoids. Furthermore, infection of organoids with recombinant HepG2.2.15 virus resulted in production of cccDNA. Inoculum that lacks cccDNA was used as a negative control for the PCR and HBV plasmid DNA was used as a positive control (Fig 3e and Supplementary Fig. 3a). To determine whether the organoids are able to produce infectious virus, supernatants containing virus produced by organoids, which were infected with recombinant HepG2.2.15 HBV were collected, concentrated and used for spinoculation of hD organoids. As shown in Fig. 3f, infection of hD organoids with organoid-produced HBV resulted in expression of intracellular HBV RNA, indicating that organoids produce infectious viral particles.

Growth of viral isolates from patient material has been limited by the lack of an adequate primary model system. However, differentiated organoids were able to support infection and replication when challenged with HBV infected patient sera, as shown by production of viral DNA, expression of viral transcripts and positive immunostaining for HBsAg (Fig. 3g and Supplementary Fig. 3b-c).This model system therefore provides a useful platform to investigate the role of specific viral factors in HBV

bioRxiv preprint doi: https://doi.org/10.1101/568147; this version posted March 5, 2019. The copyright holder for this preprint (which was not certified by peer review) is the author/funder. All rights reserved. No reuse allowed without permission.

infection. We next examined whether the ex vivo infected liver organoid platform would be amenable to drug screening according to the schematic in Fig. 3h. Infected organoids were treated with Tenofovir, a nucleoside reverse transcriptase inhibitor, which inhibits the reverse transcription of HBV pre-genomic RNA To DNA. HBV viral DNA production in the supernatant was inhibited by Tenofovir while as expected RNA levels remained the same (Fig. 3h). Thus, ex vivo infected differentiated liver organoids provide a novel primary hepatocyte platform for drug screening.

In the organoids, HBV replication, infection and spread appear to be persistent until 8 days after infection when viral production drops significantly, likely because of the limited half-life of differentiated organoids in culture (Fig. 4a). If we stimulate the proliferation or recovery of the organoids by periodically culturing the organoids in EM, extending the half-life of the infected cultures, viral production is maintained for approximately one month post infection (Supplementary Fig. 4).

As an alternative approach to improve infection efficiency, we generated transgenic hD organoids exogenously expressing NTCP under expansion conditions (Fig. 4b-d and Supplementary Fig. 5) via transduction of organoids with a lentiviral construct harboring the coding sequence of Flag-tagged NTCP ubiquitously expressed under a CMV promoter, followed by a blasticidin selection marker (Fig. 4b). Exogenous expression of NTCP in hepatoma cell lines was shown to confer susceptibility to infection[29] in line with our observed increased HBV infection in differentiated organoids, likely because of the higher level of NTCP expression. Immunofluorescence experiments performed on NTCP-liver organoids in expansion phase confirmed high levels of NTCP protein expression correctly localized to the cellular membrane (Fig. 4d and Supplementary Fig. 5b). Cholesterol target genes were induced in response to statin treatment in NTCP transgenic organoids, confirming the functionality of exogenously expressed NTCP (Supplementary Fig. 5c). However, when we then evaluated viral production after infection in NTCP organoid lines and compared it to that of the corresponding parental lines (Fig. 4e), HBV DNA and HBS antigen levels in the supernatant of NTCP-expressing organoids were similar to that of parental lines, suggesting that expression of NTCP alone is not sufficient to improve HBV infection rate in liver organoids grown in EM (Fig. 4e-f and Supplementary Fig. 5d. Differentiation of NTCP transgenic organoids led to higher levels of viral production in the supernatant (Supplementary Fig. 5d). This indicates that NTCP alone is not sufficient for HBV infection and additional factors may be necessary for optimal HBV infection of liver organoids.

bioRxiv preprint doi: https://doi.org/10.1101/568147; this version posted March 5, 2019. The copyright holder for this preprint (which was not certified by peer review) is the author/funder. All rights reserved. No reuse allowed without permission.

To obtain a long-term, expandable, primary HBV producing liver organoid model system, we generated a lentiviral construct to produce transgenic organoid lines containing an integrated copy of HBV (Fig. 4g-j and Supplementary Fig. 6). Interestingly, when the HBV genome was placed downstream of the CMV promoter, transgenic organoids, while efficiently expressing HBV RNA, did not support replication, as demonstrated by the low levels of HBV DNA in the culture supernatant (Supplementary Fig. 6d), pointing to CMV promoter-induced transcriptional interference with promoter usage required for mRNA transcription of individual HBV genes. Removal of the CMV promoter to generate "lenti-HBV" (Supplementary Fig. 6e) allowed for the generation of replication-competent, expandable, long term, hD transgenic lenti-HBV organoid lines, in which transcription from the HBV transgene results in protein and viral production (Fig. 4j and Supplementary Fig. 6e-g). Although lacking cccDNA, this model system provides a primary platform to screen for inhibitors of HBV gene expression.

Discussion

Here we present human liver organoids as a novel in vitro primary model system that supports HBV infection and replication, and which can be seeded from infected patients for molecular and functional analysis. Healthy donor liver organoids were efficiently infected with both recombinant virus as well as HBV infected patient serum, expressed HBS Ag and HBV core proteins, and produced HBV in the culture supernatant. The ex vivo infected organoid replication platform was amenable to screening for potential inhibitors of HBV replication, as we showed using the reverse transcriptase inhibitor Tenofovir. Thus the HBV infected organoid platform allows for the study of host and viral-specific factors that control the efficiency of HBV replication and viral production and provides a primary untransformed hepatocyte screening platform for discovery of candidate new drugs targeting HBV transcription and replication.

When cultured under differentiating growth conditions, the expression of the HBV receptor NTCP increased significantly in liver organoids. Consistent with the observed higher NTCP levels, in vitro infection of differentiated organoids with HBV led to higher levels of infection and replication. To mitigate the risk that long-term HBV replication would be limited by the half-life of differentiated (DM) liver organoid cultures, we generated transgenic organoids that exogenously expressed membrane localized NTCP under expansion conditions, to obtain long term HBV replicating cultures. Surprisingly, the presence of NTCP did not result in more efficient infection of organoids, suggesting that although necessary, NTCP alone may not be sufficient for optimal infection. Consistent with our

bioRxiv preprint doi: https://doi.org/10.1101/568147; this version posted March 5, 2019. The copyright holder for this preprint (which was not certified by peer review) is the author/funder. All rights reserved. No reuse allowed without permission.

observations, HepG2 cell lines exogenously expressing NTCP, while susceptible to infection are inefficiently infected with HBV and require high viral titers[29,30]. These observations are suggestive of the potential necessity for additional (co)receptors or downstream factors necessary for optimal infection in hepatocytes. In line with this notion, polyclonal lentivirally transduced liver organoids that contained integrated full length HBV genome, efficiently produced HBV under expansion conditions.

Recently alternative liver organoid model systems derived from human (induced) pluripotent stem cells[13-15,31] as well as primary human hepatocyte coculture systems[32] have been developed that can be used to study hepatitis B virus infection. However, our liver organoids constitute a unique tool and innovative approach for the molecular characterization of patient-derived HBV-induced liver disease progression and HCC; the liver organoid platform combines the ability for long-term culturing, its amenability to molecular and genetic manipulation, with the possibility to achieve a phenotype corresponding to primary hepatocytes.

Early surveillance of the changes in gene expression or biomarkers that predict the occurrence of HCC is critical to enable patients to receive timely and successful treatment. Paving the way for personalized therapy of HBV infected patients, liver organoids can be seeded from infected patient liver biopsies or resection, at different stages of the disease. Our data demonstrates that HBV infected patient-derived liver organoids are a primary cell culture model that resembles its diseased tissue of origin. Comparison of the gene expression profiles of healthy donor to HBV-infected patient-derived liver organoids, and further HDV co-infected and acute liver failure patient sub-groups point to the extent to which organoids reflect the biology and represent the transcriptomic profiles of the primary non tumor tissue of origin. The identification of early aberrant gene regulatory networks and biomarkers that drive HBV-mediated HCC, detectable at an early non-tumor stage without phenotypic signs of tumorigenesis, allows for patient-specific surveillance of disease progression and provides a screening platform for candidate drugs that guide personalized treatment by targeting early stages in HBV-mediated HCC.

bioRxiv preprint doi: https://doi.org/10.1101/568147; this version posted March 5, 2019. The copyright holder for this preprint (which was not certified by peer review) is the author/funder. All rights reserved. No reuse allowed without permission.

Materials and Methods

Liver tissue: Liver organoids from healthy donors and HBV infected patients were isolated and cultured using the method previously described by Huch et al.[20] with minor modifications. The Medical Ethical Council of the Erasmus Medical Center approved the use of this material for research purposes, and informed consent was provided from all patients. Biopsies from twelve explanted HBV infected livers and from one HBV infected donor liver were fixed for 24 hours at room temperature in 4% formaldehyde solution (Klinipath) immediately after collection in the operating room. Fixed biopsies were processed according to standard protocol to dehydrate and infiltrate with paraffin wax and subsequent embedding into paraffin blocks. Sections of 4µm were cut using a microtome and mounted on glass microscope slides. After deparaffination according to standard procedure, the tissue slides were stained with haematoxylin and eosin (Haemalum – Mayer's, VWR) according to the manufacturers protocol, dehydrated and mounted for microscopic analysis.

Isolation and culture of human liver organoids: Liver specimens (1-2 cm^3) were washed once with DMEM (Sigma) supplemented with 1% FCS and with 0.1% Penicillin Streptomycin (PS, Sigma), minced and incubated at 37°C with the digestion solution (collagenase 2.5mg/ml in HBSS). Incubation was performed for 30 minutes, further mincing and mixing the tissue every 10 minutes. To recover the cells, digestion solution was passed through a 70µM strainer in a 50 ml tube (GreinerBio) and washed with 45ml Advanced DMEM (Gibco) supplemented with 1% PS, 10mM HEPES (Gibco) and 1% GlutaMax (Gibco), henceforth Ad+++. Partially digested tissue was recovered from the strainer and further incubated with TrypLE Express (Thermoscientific) for 15 minutes at 37°C. Cells obtained from the first and second digestion were pooled together and washed twice with Ad+++. After the second centrifugation (200g, 5 minutes) cells were counted, mixed with an appropriate amount of BME solution (2/3 Basement Membrane Extract, Type 2 (Pathclear) diluted with 1/3 Ad+++) and seeded in 25µl drops containing 10000-15000 cells in 48 well suspension plates (GreinerBio). After BME solution had solidified, wells were filled with 250µl of human liver organoid isolation medium consisting Ad+++ supplemented of 1X B27 supplement without retinoic acid (Gibco), 1X N2 supplement (Gibco), 1.25mM N-acetyl-L-cysteine (Sigma), 10% (vol/vol) Rspo-1 conditioned medium[19], 10% (vol/vol) Wnt3a-conditioned medium[33], 10mM nicotinamide (Sigma), 10nM recombinant human (Leu15)-gastrin I (Sigma), 50ng/ml recombinant human EGF (Peprotech), 100ng/ml recombinant human FGF10 (Peprotech), 25ng/ml recombinant human HGF (Peprotech), 10µM Forskolin (Sigma), 5µM A8301 (Tocris), 25ng/ml Noggin (Peprotech) and 10µM Y27632

bioRxiv preprint doi: https://doi.org/10.1101/568147; this version posted March 5, 2019. The copyright holder for this preprint (which was not certified by peer review) is the author/funder. All rights reserved. No reuse allowed without permission.

(Sigma). After 1 week, isolation media was changed to human liver expansion media (EM; Ad+++ supplemented of 1X B27 supplement without retinoic acid (Gibco), 1X N2 supplement (Gibco), 1.25mM N-acetyl-L-cysteine (Sigma), 10% (vol/vol) Rspo-1 conditioned medium, 10mM nicotinamide (Sigma), 10nM recombinant human (Leu15)-gastrin I (Sigma), 50ng/ml recombinant human EGF (Peprotech), 100ng/ml recombinant human FGF10 (Peprotech), 25ng/ml recombinant human HGF (Peprotech), 10µM Forskolin (Sigma) and 5µM A8301 (Tocris))[20].

EM was changed twice a week, and cultures were split every 7-10 days according to organoid density. For passaging (1:4-1:8, depending on growth rate of the culture), organoids were resuspended in 10ml Ad+++, incubated in ice for 10 minutes and collected by centrifugation (5 minutes at 200g). Subsequently, organoids were incubated for 5 minutes in TrypLE Express at 37°C and mechanically disrupted by pipetting. After a further wash in Ad+++, cells were resuspended in BME solution and seeded in 24 or 48 wells suspension plates. After BME solution had solidified, wells were filled with 500µl (24 wells) or 250µl (48 wells) of human liver organoid expansion medium.

Hepatic differentiation of liver organoids: Human liver organoid cultures derived from healthy and HBV infected livers were seeded and cultured for 4 days in EM supplemented with 25ng/ml of BMP7 (Peprotech). Hepatic differentiation was induced by culturing human liver organoids in differentiation medium (DM; Ad+++ supplemented with 1X B27 supplement without retinoic acid, 1X N2 supplement, 1mM N-acetylcysteine, 10nM recombinant human [Leu15]-gastrin I, 50ng/ml recombinant human EGF, 25ng/ml recombinant human HGF, 0.5µM A83-01, 10µM DAPT (Sigma), 3µM dexamethasone (Sigma), 25ng/ml BMP7 and 100ng/ml recombinant human FGF19 (Peprotech)). Differentiation medium was changed twice a week for 7 days before infection or 10 days before staining for Albumin and HNF4α[20].

3' mRNA sequencing: For each RNA preparation, 2 wells of organoids in expansion phase were collected in Trizol reagent (Sigma) 4-5 days after splitting. RNA was extracted according to manufacturer's instruction and resuspended in 30µl of nuclease free water. Total RNA was quantitated (ND1000 Spectrophotometer – PEQLAB). Samples were diluted accordingly to a mean concentration of approximately 100-150ng/µl and their quality assessed on a Bioanalyzer (Agilent Technologies) using the Agilent RNA 6000 Nano Kit reagents and protocol (Agilent Technologies). RNA samples were processed for library preparation using the 3' mRNA-Seq Library Prep Kit Protocol for Ion Torrent (QuantSeq-LEXOGEN™, Vienna, Austria), according to manufacturer's instructions. Briefly, up to 500ng from each RNA sample were used for first strand synthesis. The RNA was subsequently

bioRxiv preprint doi: https://doi.org/10.1101/568147; this version posted March 5, 2019. The copyright holder for this preprint (which was not certified by peer review) is the author/funder. All rights reserved. No reuse allowed without permission.

removed and 2nd strand synthesis was initiated by a random primer, containing Ion Torrent compatible linker sequences and appropriate in-line barcodes. 2nd strand synthesis was followed by magnetic bead-based purification and the resulting library was PCR-amplified for 14 cycles and re-purified. Library quality and quantity was assessed on a Bioanalyzer using the DNA High Sensitivity Kit reagents and protocol (Agilent Technologies). The quantified libraries were pooled together at a final concentration of 100pM. The pools were templated and enriched on an Ion Proton One Touch system. Templating was performed using the Ion PI™ Hi-Q™ OT2 200 Kit (Thermo Fisher Scientific), followed by sequencing using the Ion PI™ Hi-Q™ Sequencing 200 Kit on Ion Proton PI™ V2 chips (Thermo Fisher Scientific), an Ion Proton™ System, according to the manufacturer's instructions.

Short read mapping: The Quant-Seq FASTQ files obtained from Ion Proton sequencing were mapped on the UCSC hg19 reference genome using a two-phase mapping procedure. Firstly, the short reads were mapped using tophat2[34], with the following non-default settings: --read-mismatches 3 --read-gap-length 3 --read-edit-dist 3 --no-novel-juncs, other settings at default. Additional transcript annotation data for the hg19 genome from Illumina iGenomes (http://cufflinks.cbcb.umd.edu/igenomes.html) was also provided to tophat2 for guidance. Next, the reads which remained unmapped were converted back to FASTQ files using bam2fastq from the BEDTools[35] suite and submitted to a second round of mapping using Bowtie2[36] against the hg19 genome with the --local and --very-sensitive-local switches turned on. All resulting BAM files were visualized in the UCSC Genome Browser using BEDTools and tools provided by the UCSC Genome Browser toolkit.

Statistical analysis of Quant-Seq data: The resulting Quant-Seq BAM files were analyzed with the Bioconductor package metaseqR[37] which has built-in support for Quant-Seq data. Briefly, the raw BAM files, one for each organoid sample, were summarized to a 3' UTR read counts table from Ensembl longest (dominant) transcripts (version 90). The original 3' UTR regions were extended 500bp upstream and downstream to accommodate the variable read length of Ion Proton reads. In the resulting read counts table, each row represented one 3' UTR region, each column one Quant-Seq sample and each cell the corresponding read counts associated with each row and column. The final 3' UTR read counts table was normalized for inherent systematic or experimental biases using the Bioconductor package DESeq[38] after removing areas that had zero counts over all the Quant-Seq samples. Prior to the statistical testing procedure, the 3' UTR read counts were filtered for possible artifacts that could affect the subsequent statistical testing procedures. 3' UTR areas presenting any of the following were excluded from further analysis: i) 3' UTR areas corresponding to genes smaller than

bioRxiv preprint doi: https://doi.org/10.1101/568147; this version posted March 5, 2019. The copyright holder for this preprint (which was not certified by peer review) is the author/funder. All rights reserved. No reuse allowed without permission.

500bp, ii) 3' UTRs with read counts below the median read counts of the total normalized count distribution. Similar expression thresholds (e.g. the median of the count distribution) have been previously used in the literature[39], where the authors use the median RPKM value instead of normalized counts), iii) 3' UTR areas corresponding to genes with the following Ensembl biotypes: rRNA, TR_V_pseudogene, TR_J_pseudogene, IG_C_pseudogene, IG_J_pseudogene, IG_V_pseudogene. The remaining 3' UTR counts table after filter application was subjected to differential expression analysis for the appropriate contrasts using the PANDORA algorithm implemented in metaseqR. 3' UTR areas (and their corresponding genes) presenting a PANDORA p-value less than 0.05 and fold change (for each contrast) greater than 1 or less than -1 in log2 scale were considered as differentially expressed.

Clustering analysis: Hierarchical clustering was performed using the Euclidean distance and complete linkage for the construction of the dendrograms. The expression values used to generate the heatmap were DESeq-normalized read counts in log2 scale. Multidimensional scaling was performed using the Spearman correlation distance metric on the gene expression matrix using DESeq-normalized read counts in log2 scale. All calculations and visualizations were performed using facilities from the R language. All analysis scripts and logs of the analysis pipelines are available upon request.

Gene Ontology and Pathway analysis: Gene Ontology (GO) enrichment and biochemical pathway analysis was performed using GeneCodis[40]. For the GeneCodis GO and pathway analysis the 361 iP "Signature" genes were used

Total RNA isolation and quantitative RT qPCR: RNA extraction was performed starting from 1-2 wells of a 24 wells plate, organoids were collected in 500µl of cell lysis buffer and processed using RealiaPrep RNA Cell Miniprep System (Promega), according to manufacturer's instructions. cDNA synthesis was performed starting from 300-1000ng of RNA using Superscript II Reverse Transcriptase (Life Technologies) kit following manufacturer's protocol for random primer cDNA synthesis. cDNA was diluted 1:5 in nuclease free water and 2µl of the diluted product was used for real time PCR with the following reagents: 5µl of GoTaq qPCR Master Mix (Promega), 2µl of nuclease free water and 1µl of 10mM primer mix. Amplification was performed on the CFX Connect Real-Time PCR Detection System thermocycler (BioRad) using following thermal program starting with 3 minutes at 95°C, followed by 40 cycles of 95°C for 10 seconds and 60°C for 30 seconds. Specificity of the RT-qPCR products was assessed by melting curve analysis. Primers used for real-time qPCR are listed below.

GAPDH Fwd 5'-CAAGAAGGTGGTGAAGCAG-3'; Rev 5'-GCCAAATTCGTTGTCATACC-3'

bioRxiv preprint doi: https://doi.org/10.1101/568147; this version posted March 5, 2019. The copyright holder for this preprint (which was not certified by peer review) is the author/funder. All rights reserved. No reuse allowed without permission.

KRT7 Fwd 5'-CTCCGGAATACCCGGAATGAG-3'; Rev 5'-ATCACAGAGATATTCACGGCTCC-3'

CYP3A4 Fwd 5'-TGTGCCTGAGAACACCAGAG-3'; Rev 5'-GTGGTGGAAATAGTCCCGTG-3'

NTCP Fwd 5'-GCTTTCTGCTGGGTTATGTTCTC-3'; Rev 5'-CATCCAGTCTCCATGCTGACA-3'

HNF4A Fwd 5'-CGTGCTGCTCCTAGGCAATGAC-3'; Rev 5'-ACGGACCTCCCAGCAGCATCT-3'

SOX9 Fwd 5'-GGAAGTCGGTGAAGAACGGG-3'; Rev 5'-TGTTGGAGATGACGTCGCTG-3'

ALBUMIN Fwd 5'-GCGACCATGCTTTTCAGCTC-3'; Rev 5'-GTTGCCTTGGGCTTGTGTTT-3'

LGR5 Fwd 5'-AGGTCTGGTGTGTTGCTGAGG-3'; Rev 5'-TGAAGACGCTGAGGTTGGAAGG-3'

LDLR Fwd 5'-GACGTGGCGTGAACATCTG-3'; Rev 5'-CTGGCAGGCAATGCTTTGG-3'

PCSK9 Fwd 5'-AGGGGAGGACATCATTGGTG-3'; Rev 5'-CAGGTTGGGGGTCAGTACC-3'

Gene expression levels were calculated using the 2ΔCt method, whereas fold increase was calculated using the 2ΔΔCt[41]. GAPDH was used as housekeeping control.

Immunofluorescence and image analysis: Human liver organoids were collected and washed three times to with cold Ad+++ to remove BME, then fixed with 4% paraformaldehyde for 30 minutes in ice and permeabilized using 0.3% (HBcAg, HNF4α and NTCP) or 1% (Albumin) Triton X-100 (Sigma) in PBS for 30 minutes at room temperature. For HBsAg staining cells were fixed and permeabilized in 100% Acetone. Specimens were incubated for 2h at room temperature in PBS plus 10% BSA (Roche) and 0.5% FCS (HBsAg) or PBS plus 0.5% FCS, 0.3% triton, 1% BSA 1%DMSO (Albumin, HBcAg, HNF4α and SLC10A1). Following blocking, human liver organoids were incubated overnight with primary antibodies (mouse anti-HBcAg, mouse anti- HBsAg (ThermoScientific), goat anti-Albumin, rabbit anti-HNF4α (Santa Cruz Biotechnology) and rabbit anti-SLC10A1 (NTCP, Sigma) diluted in PBS + 10% blocking buffer. After extensive washing, human liver organoids were stained with appropriate Alexa Fluor dye-conjugated secondary antibodies (Life Technologies). Nuclei were stained with Hoechst33342 (Molecular Probes). Immunofluorescence images were acquired using a confocal microscope (Leica, SP5). Images were analyzed and processed using Leica LAS AF Lite software (Leica SP5 confocal). All phase contrast pictures were acquired using a Leica DMIL microscope and a DFC420C camera.

Production of HBV virus and HBV infection: HepG2.2.15 cells, a HepG2 derived cells line stably transfected with full length HBV (kindly provided by Prof. Bart Haagmans, Erasmus MC) were cultured in DMEM medium (Gibco) supplemented with 10% fetal bovine serum (Gibco) and 1%

bioRxiv preprint doi: https://doi.org/10.1101/568147; this version posted March 5, 2019. The copyright holder for this preprint (which was not certified by peer review) is the author/funder. All rights reserved. No reuse allowed without permission.

penicillin/streptomycin. For virus production, $3x10^6$ cells were plated in collagen coated 10cm plates, cultured in supplemented DMEM until confluency and subsequently in Ad+++ for 4 days. The supernatant of HepG2.2.15 cells was then collected, filtered and concentrated using the PEG Virus Precipitation Kit (Abcam) following the manufacturer's instructions. Precipitated virus was aliquoted and stored at -80°C until use. Human serum was obtained from residual samples from HBV infected individuals attending Erasmus MC for routine clinical activity. As negative control, an aliquot of the virus equivalent to the inoculum was inactivated by incubation at 100°C for 30 minutes. Human liver organoids were resuspended using either active virus or heat inactivated control, transferred to 24 wells plate and centrifugated for 1h at 600g. Following spinoculation, plates were incubated at 37°C for 5h and then seeded in BME following the culturing protocol. After BME solution has solidified, liver organoids were maintained in EM for 16h, washed 4 times with Ad+++ and cultured EM or DM as indicated.

Detection of HBV DNA and RNA: DNA was extracted from culture supernatants using the QIAamp MinElute Virus Spin Kit following manufacturer's instructions. DNA extracted from supernatant and cDNA obtained from reverse transcription of intracellular DNA (see section 9 for details) were analyzed in duplicate using a TaqMan based qPCR assay. For each reaction, a 25ul mixture was prepared containing 2.5µl 10X Buffer, 1.75µl 25mM MgCl2, 1µl 10mM dNTPs, 1U of Platinum Taq, 0.125µl of 100µM forward (5'-GCAACTTTTTCACCTCTGCCT A-3') and reverse primer (5'-AGTAACTCCACAGTAGCTCCAAATT-3'), 0.075µl of 50µM probe (FAM-TTCAAGCCTCCAAGCTGTGCCTTGGGTGGC-TAMRA), and 7.5µl (DNA) or 4µl (cDNA) of template. Each PCR reaction included a standard curve made of dilutions of a plasmid containing the full-length HBV genome ranging from 4 to $4x10^5$ copies of plasmid. Beta-2-microglobulin was used as housekeeping control for expression analysis of cDNA samples (B2M Fwd 5'-AGCGTACTCCAAAGATTCAGGTT-3', B2M Rev 5'-ATGATGCTGCTTACATGTCTCGAT-3', B2M probe FAM-TCCATCCGACATTGAAGTTGACTTACTG-BHQ1).

Detection of pol and HBX transcripts was performed using a previously published nested PCR protocol[42].

Isolation and detection of HBV cccDNA from infected liver organoids: HBV cccDNA was isolated from HBV and HI (negative control) infected human liver organoids by a previously described alkali lysis plasmid DNA isolation protocol with a minor modification[43]. Briefly, Human liver organoids were collected on day 8 post infection incubated on ice for 10-20 mins and washed with Ad+++ to

bioRxiv preprint doi: https://doi.org/10.1101/568147; this version posted March 5, 2019. The copyright holder for this preprint (which was not certified by peer review) is the author/funder. All rights reserved. No reuse allowed without permission.

remove the BME. After centrifugation (5 mins at 1000rpm) organoids were treated with TrypLE Express and incubated for 30-50 sec at room temperature. Organoids were washed with PBS and collected by centrifugation (5 mins at 1000rpm), resuspended with 800µl of ice-cold cell lysis buffer (1mM EDTA (pH 8.0), 5mM Tris: HCl (pH 7.5) and 0.05% Nonidet P-40). After 10 min incubation on ice, an equal volume of alkali lysis buffer (0.1M NaOH, 6% SDS) was added and the solution was incubated for 30 mins at 37°C. DNA was neutralized by adding 3M potassium acetate (pH 5.0) to a final concentration of 0.6M and centrifuged for 5 mins at 12000 rpm. The supernatant was extracted two times with phenol followed by extraction with butanol: isopropanol (7:3) for removal of residual phenol. Subsequently, the DNA was precipitated with 1ml 100% ethanol, 400µl 7.5M ammonium acetate and 1µl 20mg/ml glycogen overnight at -80°C. Next day, the cccDNA sample was spun down for 30 mins at 4°C, 14000 rpm and washed with 70% ethanol. After spinning the samples for 15 mins at 4°C, 14000 rpm, the pellet was resuspended in 50µl of nuclease free water.

To remove the chromosomal DNA or any linear HBV DNA, 25µl of the isolated HBV cccDNA, HBV plasmid (positive control) and HBV DNA from inoculum was digested with plasmid-safe DNase (Epicentre, E3101K, Madison, WI). According to the manufacturer's protocol, the samples were digested for 1 hr at 37°C followed by 30 mins of heat inactivation at 70°C. The digested samples were diluted 1:8 with nuclease free water.

For quantification of cccDNA a TaqMan based qPCR was performed, whereby for each reaction 20µl reaction-mix was prepared containing 4.2µl of the diluted cccDNA, 10µl LightCycler®480 Probes Master (Roche), 1µM primer mix (Fwd 5'-GTCTGTGCCTTCTCATCTGC-3'; Rev 5'-AGTAACTCCACAGTAGCTCCAAATT-3'), 0.2µM probe (FAM-TTCAAGCCTCCAAGCTGTGCCTTGGGTGGC-BHQ1) and 4% DMSO. qPCR was carried out using a previously published protocol 95°C for 10□min, followed by 50 cycles of 95°C for 15□s, and 61°C for 1□min[44].

Infection with HBV generated from organoids: the supernatant produced by infected organoids at 4-8 days post infection was collected and concentrated using Amicon Ultra-15 100K (Milipore). Human liver organoids were resuspended using either concentrated HBV virus or HI control. After an hour of spinoculation at 32°C 600g, plate was incubated at 37°C overnight and then washed & seeded in BME following the HBV infection and culturing protocol.

Generation of the lentiviral vectors and transduction of liver organoids: A gene block fragment encoding human NTCP was designed based on the reference sequence retrieved from NCBI nucleotide

bioRxiv preprint doi: https://doi.org/10.1101/568147; this version posted March 5, 2019. The copyright holder for this preprint (which was not certified by peer review) is the author/funder. All rights reserved. No reuse allowed without permission.

database (NM_003049.3). A 3X Flag PCR fragment including NTCP coding sequence was amplified using the NTCP_FWD (CACCATGGATTACAAGGATGACGACGATAAGGATTACAAGGATGACGACGATAAGGATTACAAGGATGACGACGATAAGATGGAGGCCCACAACGCGTCTgcccca) and NTCP_REV (TTACTAGGCTGTGCAAGGGGAGCA) primers and cloned in the pENTR/D-TOPO entry vector (Invitrogen) following manufacturer's instructions.

A pENTR/D-TOPO vector harboring a competent full-length copy of HBV (1.3 wt genomes) was generated using a Gibson Assembly protocol. Two fragments encompassing 1.3 times the wt HBV genome were purified using the QIAquick PCR Purification Kit (Qiagen) after PCR using the following primer pairs: VectorFwd (5'-caaaaaagcaggctccgcggccgcccccttcacGGACGACCCTTCTCGGGG-3')/MiddleRev (5'-gagaagtccaccacgAGTCTAGACTCTGCGGTATTGTGAG-3') and MiddleFwd (5'-cgcagagtctagactCGTGGTGGACTTCTCTCAATTTTC-3')/ VectorRev (5'-tgccaactttgtacaagaaagctgggtcggAGGGGCATTTGGTGGTCTATAAG-3'). The HepG2.2.15 DNA was used as template for the PCR: An empty pENTR/D-TOPO was cut with NotI and BssHI and gel purified using QIAquick Gel Extraction Kit (Qiagen). After purification, the entry vector and the PCR fragments were assembled using the Gibson Assembly Master Mix (New England BioLabs), following manufacturer's instructions.

To generate lentiviral constructs, the fragments cloned into entry vectors were transferred to a lentiviral expression destination vector (pLenti6/V5-DEST Gateway Vector, Invitrogen), using the Gateway technology (Invitrogen). The full-length HBV pLenti6/V5-DEST vector was further modified in order to remove the CMV promoter. The vector was digested with two restriction enzymes flanking the CMV promoter, ClaI and PstI (New England Biolabs), and purified from gel using QIAquick Gel Extraction Kit. After filling end gaps using Klenow polymerase (New England Biolabs), plasmids were ligated and transformed in One Shot® Stbl3™ Chemically Competent E. coli (Invitrogen). All HBV and NTCP lentiviral vectors were sequenced to verify vector structure and integrity of open reading frames.

The lentiviral constructs were generated using the ViraPower Kit (Invitrogen) and 293FT cells, following manufacturer's protocol. Briefly, one day prior transfection, $3x10^5$ cells were plated in 10cm dishes in DMEM + 10% FCS. The following day, DMEM was replaced with 5ml of Opti MEM I (Invitrogen) and cells were transfected with 9µg of the ViraPower Packaging Mix and 3µg of the pLenti6/V5-DEST Gateway Vector using Lipofectamine (Invitrogen). The day after transfection media

bioRxiv preprint doi: https://doi.org/10.1101/568147; this version posted March 5, 2019. The copyright holder for this preprint (which was not certified by peer review) is the author/funder. All rights reserved. No reuse allowed without permission.

was changed to DMEM + 10% FCS. Cell supernatant containing the lentiviral particles was collected 60 and 72 hours after transfection, filtered with a 0.42µm filter, aliquoted and stored at -80°C.

Early passage (passage 0 to 3) human liver organoids were collected in cold Ad+++ and incubate for 10 minutes in ice to remove BME. After centrifugation (5 minutes at 200g), organoids were resuspended in TrypLE Express and incubated until single cells were >80%. Cells were collected by centrifugation (5 minutes at 200g), resuspended in 1ml of lentiviral harvest and divided over 4 wells of a 48 wells plate. Plates were centrifugated for 1h at 600g and then incubated for 5h at 37°C. Afterwards, cells were collected by centrifugation (5 minutes at 200g), resuspended in BME solution and plated. After BME has solidified, wells were filled with EM supplemented with 25ng/ml Noggin and 10µM Y27632. Four days after infection medium was changed to EM supplemented with 25ng/ml Noggin and 10µM Y27632 and 5ug/ml blasticidin. Organoids were kept under selection for 7 days and then media was changed to regular EM. Once selected organoids have recovered, cultures were splitted to remove dead cells and cultured according to the regular protocol. Parallel infections were performed using HepG2 cells and the same lentiviral constructs in order to generate control cell lines.

To determine NTCP functionality following transduction with NTCP lentiviral vector, parental and selected NTCP transduced organoids were cultured in EM or EM supplemented with different concentrations of Aruvastatin and Rosuvastatin for 12h. Organoids from 2 wells of a 24 wells plate were collected in 500µl of cell lysis buffer and processed using RealiaPrep RNA Cell Miniprep System (Promega), according to manufacturer's instructions.

To determine HBV production following transduction with full length HBV lentiviral vector, supernatant and cells from transduced cultures were collected at different time points after completion of blasticidin selection. Presence of viral DNA in the supernatant and cellular associated viral RNA was assessed using the real time protocol detailed in section 11. Presence of HBsAg in organoid supernatant was assessed using the MonaLisa Kit (Promega) according to manufacturer's instructions.

Data availability:

Sequencing data that support the findings of this study have been deposited in GEO with the accession code GSE 126798.

bioRxiv preprint doi: https://doi.org/10.1101/568147; this version posted March 5, 2019. The copyright holder for this preprint (which was not certified by peer review) is the author/funder. All rights reserved. No reuse allowed without permission.

Acknowledgments

We would like to thank Vaggelis Harokopos for NGS and Karien Hamer for technical support.

Conflicts of interest

TM received funding from the European Research Council (ERC) under the European Union's Seventh Framework Programme (FP/2007-2013)/ERC STG 337116 Trxn-PURGE, Dutch AIDS Fonds grants 2014021 and 2016014, and Erasmus MC mRACE research grant. EDC received funding from Bristol Meyers Squibb (Partnering for the cure program).

Author Contributions

EDC, FC, MMK, SR, TWK, FP and TM carried out the experiments and performed data analysis. PM, CK, RJP, and PH performed RNAseq and gene expression analysis. MMA, LVDL, JMNI, CB provided tissue samples and serum from HBV infected patients. FP, MMA, LVDL, CB, HG, MH, SFB, RV, HC, and provided expertise, material and contributed to the writing of the manuscript. EDC, FC, RV, PH and TM conceived the study and wrote the manuscript. All authors read and approved the final manuscript.

bioRxiv preprint doi: https://doi.org/10.1101/568147; this version posted March 5, 2019. The copyright holder for this preprint (which was not certified by peer review) is the author/funder. All rights reserved. No reuse allowed without permission.

References

1 Thomas, E., Yoneda, M. & Schiff, E. R. Viral hepatitis: past and future of HBV and HDV. *Cold Spring Harb Perspect Med* **5**, a021345, doi:5/2/a021345 [pii]10.1101/cshperspect.a021345 (2015).

2 El-Serag, H. B. Epidemiology of viral hepatitis and hepatocellular carcinoma. *Gastroenterology* **142**, 1264-1273 e1261, doi:S0016-5085(12)00220-X [pii]10.1053/j.gastro.2011.12.061 (2012).

3 Jiang, Z. *et al.* The effects of hepatitis B virus integration into the genomes of hepatocellular carcinoma patients. *Genome Res* **22**, 593-601 (2012).

4 Fattovich, G., Bortolotti, F. & Donato, F. Natural history of chronic hepatitis B: special emphasis on disease progression and prognostic factors. *J Hepatol* **48**, 335-352, doi:S0168-8278(07)00637-X [pii]10.1016/j.jhep.2007.11.011 (2008).

5 Ji, X. *et al.* Somatic mutations, viral integration and epigenetic modification in the evolution of hepatitis B virus-induced hepatocellular carcinoma. *Curr Genomics* **15**, 469-480 (2014).

6 Sung, W. K. *et al.* Genome-wide survey of recurrent HBV integration in hepatocellular carcinoma. *Nat Genet* **44**, 765-769 (2012).

7 Fujimoto, A. *et al.* Whole-genome sequencing of liver cancers identifies etiological influences on mutation patterns and recurrent mutations in chromatin regulators. *Nat Genet* **44**, 760-764, doi:ng.2291 [pii]10.1038/ng.2291 (2012).

8 Huang, J. *et al.* Exome sequencing of hepatitis B virus-associated hepatocellular carcinoma. *Nat Genet* **44**, 1117-1121, doi:ng.2391 [pii]10.1038/ng.2391 (2012).

9 Shibata, T. & Aburatani, H. Exploration of liver cancer genomes. *Nat Rev Gastroenterol Hepatol* **11**, 340-349 (2014).

10 Cancer Genome Atlas Research Network. Electronic address, w. b. e. & Cancer Genome Atlas Research, N. Comprehensive and Integrative Genomic Characterization of Hepatocellular Carcinoma. *Cell* **169**, 1327-1341 e1323 (2017).

11 Zhang, X.-D., Wang, Y. & Ye, L.-H. Hepatitis B virus X protein accelerates the development of hepatoma. *Cancer biology & medicine* **11**, 182-190, doi:10.7497/j.issn.2095-3941.2014.03.004 (2014).

12 Thomas, E. & Liang, T. J. Experimental models of hepatitis B and C - new insights and progress. *Nat Rev Gastroenterol Hepatol* **13**, 362-374, doi:nrgastro.2016.37 [pii]10.1038/nrgastro.2016.37 (2016).

13 Nie, Y. Z. *et al.* Recapitulation of hepatitis B virus-host interactions in liver organoids from human induced pluripotent stem cells. *EBioMedicine* **35**, 114-123 (2018).

14 Sakurai, F. *et al.* Human induced-pluripotent stem cell-derived hepatocyte-like cells as an in vitro model of human hepatitis B virus infection. *Sci Rep* **7**, 45698 (2017).

15 Kaneko, S. *et al.* Human induced pluripotent stem cell-derived hepatic cell lines as a new model for host interaction with hepatitis B virus. *Sci Rep* **6**, 29358 (2016).

16 Wilkening, S., Stahl, F. & Bader, A. Comparison of primary human hepatocytes and hepatoma cell line Hepg2 with regard to their biotransformation properties. *Drug Metab Dispos* **31**, 1035-1042 (2003).

17 Guillouzo, A. *et al.* The human hepatoma HepaRG cells: a highly differentiated model for studies of liver metabolism and toxicity of xenobiotics. *Chem Biol Interact* **168**, 66-73, doi:S0009-2797(06)00355-3 [pii]10.1016/j.cbi.2006.12.003 (2007).

18 Kidambi, S. *et al.* Oxygen-mediated enhancement of primary hepatocyte metabolism, functional polarization, gene expression, and drug clearance. *Proc Natl Acad Sci U S A* **106**, 15714-15719 (2009).

19 Huch, M. *et al.* In vitro expansion of single Lgr5+ liver stem cells induced by Wnt-driven regeneration. *Nature* **494**, 247-250, doi:nature11826 [pii]10.1038/nature11826 (2013).

20 Huch, M. *et al.* Long-term culture of genome-stable bipotent stem cells from adult human liver. *Cell* **160**, 299-312, doi:S0092-8674(14)01566-9 [pii]10.1016/j.cell.2014.11.050 (2015).

21 Broutier, L. *et al.* Human primary liver cancer-derived organoid cultures for disease modeling and drug screening. *Nat Med* **23**, 1424-1435, doi:nm.4438 [pii]10.1038/nm.4438 (2017).

22 Allain, C., Angenard, G., Clement, B. & Coulouarn, C. Integrative Genomic Analysis Identifies the Core Transcriptional Hallmarks of Human Hepatocellular Carcinoma. *Cancer Res* **76**, 6374-6381 (2016).

23 Gao, W. *et al.* Variable DNA methylation patterns associated with progression of disease in hepatocellular carcinomas. *Carcinogenesis* **29**, 1901-1910 (2008).

24 Paradis, V. *et al.* Molecular profiling of hepatocellular carcinomas (HCC) using a large-scale real-time RT-PCR approach: determination of a molecular diagnostic index. *Am J Pathol* **163**, 733-741 (2003).

25 Chen, Y. *et al.* MicroRNA-1271 functions as a potential tumor suppressor in hepatitis B virus-associated hepatocellular carcinoma through the AMPK signaling pathway by binding to CCNA1. *J Cell Physiol* **234**, 3555-3569 (2019).

bioRxiv preprint doi: https://doi.org/10.1101/568147; this version posted March 5, 2019. The copyright holder for this preprint (which was not certified by peer review) is the author/funder. All rights reserved. No reuse allowed without permission.

26 Tao, R. *et al*. Methylation profile of single hepatocytes derived from hepatitis B virus-related hepatocellular carcinoma. *PLoS One* **6**, e19862 (2011).

27 Ashida, R. *et al*. CYP3A4 Gene Is a Novel Biomarker for Predicting a Poor Prognosis in Hepatocellular Carcinoma. *Cancer Genomics Proteomics* **14**, 445-453 (2017).

28 Yamaguchi, M. Involvement of regucalcin as a suppressor protein in human carcinogenesis: insight into the gene therapy. *J Cancer Res Clin Oncol* **141**, 1333-1341 (2015).

29 Yan, H. *et al*. Sodium taurocholate cotransporting polypeptide is a functional receptor for human hepatitis B and D virus. *Elife* **1**, e00049 (2012).

30 Iwamoto, M. *et al*. Evaluation and identification of hepatitis B virus entry inhibitors using HepG2 cells overexpressing a membrane transporter NTCP. *Biochem Biophys Res Commun* **443**, 808-813 (2014).

31 Xia, Y. *et al*. Human stem cell-derived hepatocytes as a model for hepatitis B virus infection, spreading and virus-host interactions. *J Hepatol* **66**, 494-503 (2017).

32 March, S. *et al*. Micropatterned coculture of primary human hepatocytes and supportive cells for the study of hepatotropic pathogens. *Nat Protoc* **10**, 2027-2053 (2015).

33 Barker, N. *et al*. Lgr5(+ve) stem cells drive self-renewal in the stomach and build long-lived gastric units in vitro. *Cell Stem Cell* **6**, 25-36 (2010).

34 Kim, D. *et al*. TopHat2: accurate alignment of transcriptomes in the presence of insertions, deletions and gene fusions. *Genome Biol* **14**, R36 (2013).

35 Quinlan, A. R. & Hall, I. M. BEDTools: a flexible suite of utilities for comparing genomic features. *Bioinformatics* **26**, 841-842 (2010).

36 Langmead, B. & Salzberg, S. L. Fast gapped-read alignment with Bowtie 2. *Nat Methods* **9**, 357-359 (2012).

37 Moulos, P. & Hatzis, P. Systematic integration of RNA-Seq statistical algorithms for accurate detection of differential gene expression patterns. *Nucleic Acids Res* **43**, e25 (2015).

38 Anders, S., Reyes, A. & Huber, W. Detecting differential usage of exons from RNA-seq data. *Genome Res* **22**, 2008-2017 (2012).

39 Mokry, M. *et al*. Integrated genome-wide analysis of transcription factor occupancy, RNA polymerase II binding and steady-state RNA levels identify differentially regulated functional gene classes. *Nucleic Acids Res* **40**, 148-158 (2012).

40 Tabas-Madrid, D., Nogales-Cadenas, R. & Pascual-Montano, A. GeneCodis3: a non-redundant and modular enrichment analysis tool for functional genomics. *Nucleic Acids Res* **40**, W478-483 (2012).

41 Schmittgen, T. D. & Livak, K. J. Analyzing real-time PCR data by the comparative C(T) method. *Nat Protoc* **3**, 1101-1108 (2008).

42 Wong, D. K. *et al*. Occult hepatitis B infection and HBV replicative activity in patients with cryptogenic cause of hepatocellular carcinoma. *Hepatology* **54**, 829-836 (2011).

43 Yang, W., Mason, W. S. & Summers, J. Covalently closed circular viral DNA formed from two types of linear DNA in woodchuck hepatitis virus-infected liver. *J Virol* **70**, 4567-4575 (1996).

44 Winer, B. Y. *et al*. Long-term hepatitis B infection in a scalable hepatic co-culture system. *Nat Commun* **8**, 125 (2017).

bioRxiv preprint doi: https://doi.org/10.1101/568147; this version posted March 5, 2019. The copyright holder for this preprint (which was not certified by peer review) is the author/funder. All rights reserved. No reuse allowed without permission.

Fig. 1. Characterization of organoid cultures from liver explants of HBV-infected patients. (A) Representative panel showing the procedure to generate organoid cultures from liver tissue. (B) Hematoxylin-eosin stained sections of explanted liver tissue and phase contrast pictures showing the morphology of liver organoids derived from HBV infected individuals. (C) Expression profile of the progenitor markers LGR5, KRT7, HNF4α, and Sox9 in EM (undifferentiated) organoids derived from liver of healthy donors (hD) (n=4) and HBV infected individuals (iP) (n=5). Levels of expression were calculated according to the 2ΔCT method using GAPDH as reference gene (D) Differentiation capacity of organoid cultures derived from liver of hDs (n=4) and iPs (n=5). Bars represents fold difference in the expression of hepatocyte specific genes Albumin, Cytochrome C 3A4, NTCP and of the progenitor specific gene LGR5 in DM (differentiated) cultures compared to EM organoids using the 2ΔΔCT method. (E). Immunofluorescent staining targeting albumin (green) and HNF4α (red) was performed in EM and DM organoids. Phase contrast images, depicting the morphology of the cells are shown as reference. (F) Hierarchical clustering heatmap of differentially expressed genes derived from the comparison between the group of five hDs and five iPs presenting HBV infection and HCC (four out of five).

bioRxiv preprint doi: https://doi.org/10.1101/568147; this version posted March 5, 2019. The copyright holder for this preprint (which was not certified by peer review) is the author/funder. All rights reserved. No reuse allowed without permission.

Fig. 2. Identification of early HCC gene signature in non-tumor iP-derived organoids. (A) Box plot of DESeq normalized counts of 33 putative biomarker genes obtained from healthy donor organoids (depicted in green) or obtained from HBV-iP organoids (depicted in red). (B) Hierarchical clustering heatmap of all iP and hD samples depicting the grouping and expression levels of protein coding differentially expressed genes derived from the comparison between the group of five hDs and five iPs presenting HBV infection and HCC (four out of five). Coloured bars on top of the heatmap indicate HBV status (black for HBV positive patients, gray for healthy donors), disease status (red for HBV positive HCC, orange for HBV positive without HCC, blue for HBV positive acute liver failure, green for healthy donors), and HDV coinfection status (purple HBV positive HDV negative, light blue for HBV positive HDV positive, yellow for healthy donors). (C) Multidimensional scaling plot of all iP and hD samples. (D) Hierarchical clustering heatmap of liver HCC gene expression data from 342 HCC tissue samples and 47 samples from matched nearby tissue from TCGA using the HBV iP versus hD gene signature from 1F.

bioRxiv preprint doi: https://doi.org/10.1101/568147; this version posted March 5, 2019. The copyright holder for this preprint (which was not certified by peer review) is the author/funder. All rights reserved. No reuse allowed without permission.

Fig. 3: Modeling HBV infection in vitro using human liver organoids (A) Experimental design of infection experiments. Arrows indicate the time points for HBV detection. (B) Levels of HBV DNA in supernatant of infected organoid cultures were quantified by real time PCR and compared to the cultures challenged with HI virus. (C) Schematics of the HBV genome showing ORFs (arrows) and the localization of PCR products (blue boxes). The agarose gel shows the results of the nested PCR performed on cDNA obtained from two different hD organoid lines infected in vitro. (D) Immunofluorescent stainings showing the expression of HBcAg (green) together with NTCP (magenta) or HNF4α (red) performed in undifferentiated (EM) and differentiated (DM) hD organoids 6 days after HBV infection. (E) Quantification of total HBV DNA (orange) and cccDNA (green) from supernatant of infected organoids (inoculum), from double stranded HBV plasmid (as positive control), and from DNA purified from organoids 8 days post infection. (F) Organoids produce infectious HBV: Expression of intracellular HBV RNA is shown relative to beta 2 microglobulin in organoids infected with organoid produced HBV. (G) Immunofluorescent staining showing the expression of HBsAg (green) in DM organoids infected with recombinant HBV and patient serum. Scale bars represent 50 µm. Bar graphs show total HBV RNA levels in the culture at the time of staining. (H) Experimental design of Tenofovir treatment of infected organoids. Levels of HBV DNA in the supernatant and intracellular HBV RNA were quantified by real time PCR and RT-PCR respectively.

bioRxiv preprint doi: https://doi.org/10.1101/568147; this version posted March 5, 2019. The copyright holder for this preprint (which was not certified by peer review) is the author/funder. All rights reserved. No reuse allowed without permission.

Fig. 4: Long term HBV producing transgenic liver organoid model Modeling (A) Levels of HBV DNA in supernatant of differentiated organoid cultures over time. Panels above the timeline arrow show representative pictures of the culture at the indicated time points (B) Schematic representation of the experimental procedure for the transduction experiments. Following infection with a lentiviral vector expressing Flag-NTCP, organoids were selected with blasticidin for 5 days in order to obtain lines expressing NTCP in the expansion phase. (C) Levels of expression of NTCP were evaluated by RT-PCR in the untransduced (Parental) and the transduced (NTCP) lines. Expression of NTCP was calculated according to the 2ΔCt method using the housekeeping gene GAPDH as reference gene and confirmed by immunofluorescence staining targeting NTCP (magenta) or Flag (red) (D). (E) HBV DNA in the supernatant of NTCP expressing organoids cultures was quantified 5 days after infection and compared to DNA detected in the supernatant of untransduced HBV infected organoids. Bars represent fold increase in HBV DNA detected in the supernatant, untransduced HBV infected organoids were used as reference. (F) HBsAg released in the supernatant of hD15 parental and NTCP organoid lines grown in EM or DM 10 days after HBV infection was detected by ELISA. Challenge with heat inactivated virus was used to control for HBsAg present in the inoculum. Pos and neg bars correspond to positive and negative controls provided by the kit manufacturer. Threshold for positivity (red line) was calculated as the average OD + 2SD of negative controls. (G-H-I) Experimental procedure for the generation of transgenic organoid lines expressing full length HBV. EM organoids were infected with a lentiviral vector including a construct encoding 1.3 copies of the HBV genome and selected with blasticidin for 5 days in order to obtain stable transgenic organoid lines. (J) Viral production was determined by real time PCR, measuring the amount of HBV DNA secreted in the supernatant at regular intervals and up to 62 days after lentiviral infection.

bioRxiv preprint doi: https://doi.org/10.1101/568147; this version posted March 5, 2019. The copyright holder for this preprint (which was not certified by peer review) is the author/funder. All rights reserved. No reuse allowed without permission.

Supplementary Materials

Figure S1: iP derived and hD derived organoids have comparable differentiation potential

Figure S2: Differentiated organoids express higher levels of NTCP

Figure S3: HBV specific RNA and proteins are detected in hD derived organoids upon infection with recombinant HBV virus as well as with HBV patient's serum.

Figure S4: Release of HBV DNA declines over time in hD organoid lines infected in vitro

Figure S5: hD organoid lines expressing high levels of functional NTCP can be generated by lentiviral infection

Figure S6: Generation of lentiviral construct used to establish human liver organoid lines expressing viral RNA and releasing virus in the supernatant.

Table S1: Characteristics of patients included in the study

Table S2: Gene expression signature

Table S3: GO analysis

bioRxiv preprint doi: https://doi.org/10.1101/568147; this version posted March 5, 2019. The copyright holder for this preprint (which was not certified by peer review) is the author/funder. All rights reserved. No reuse allowed without permission.

Fig. 1

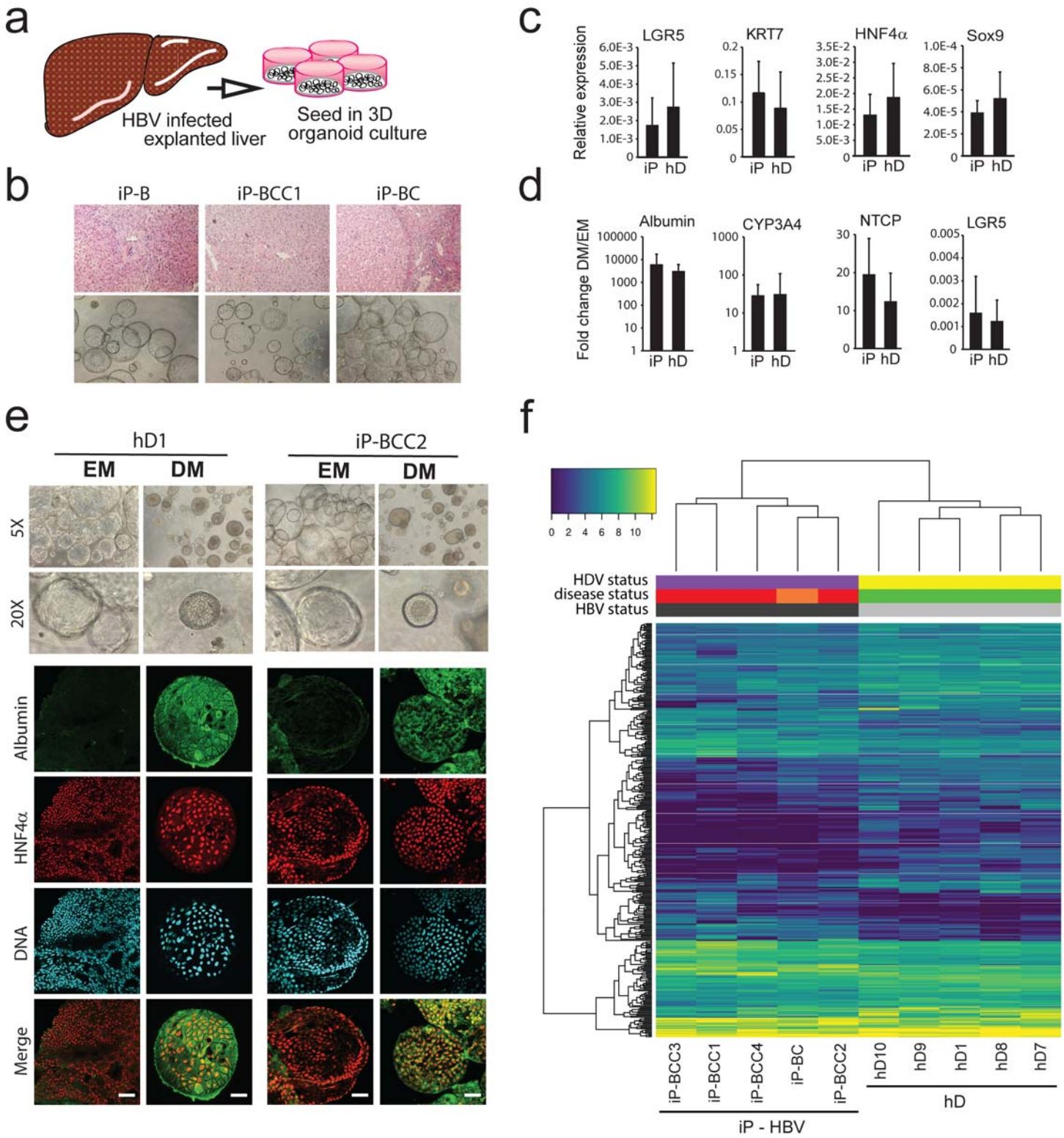

bioRxiv preprint doi: https://doi.org/10.1101/568147; this version posted March 5, 2019. The copyright holder for this preprint (which was not certified by peer review) is the author/funder. All rights reserved. No reuse allowed without permission.

Fig. 2

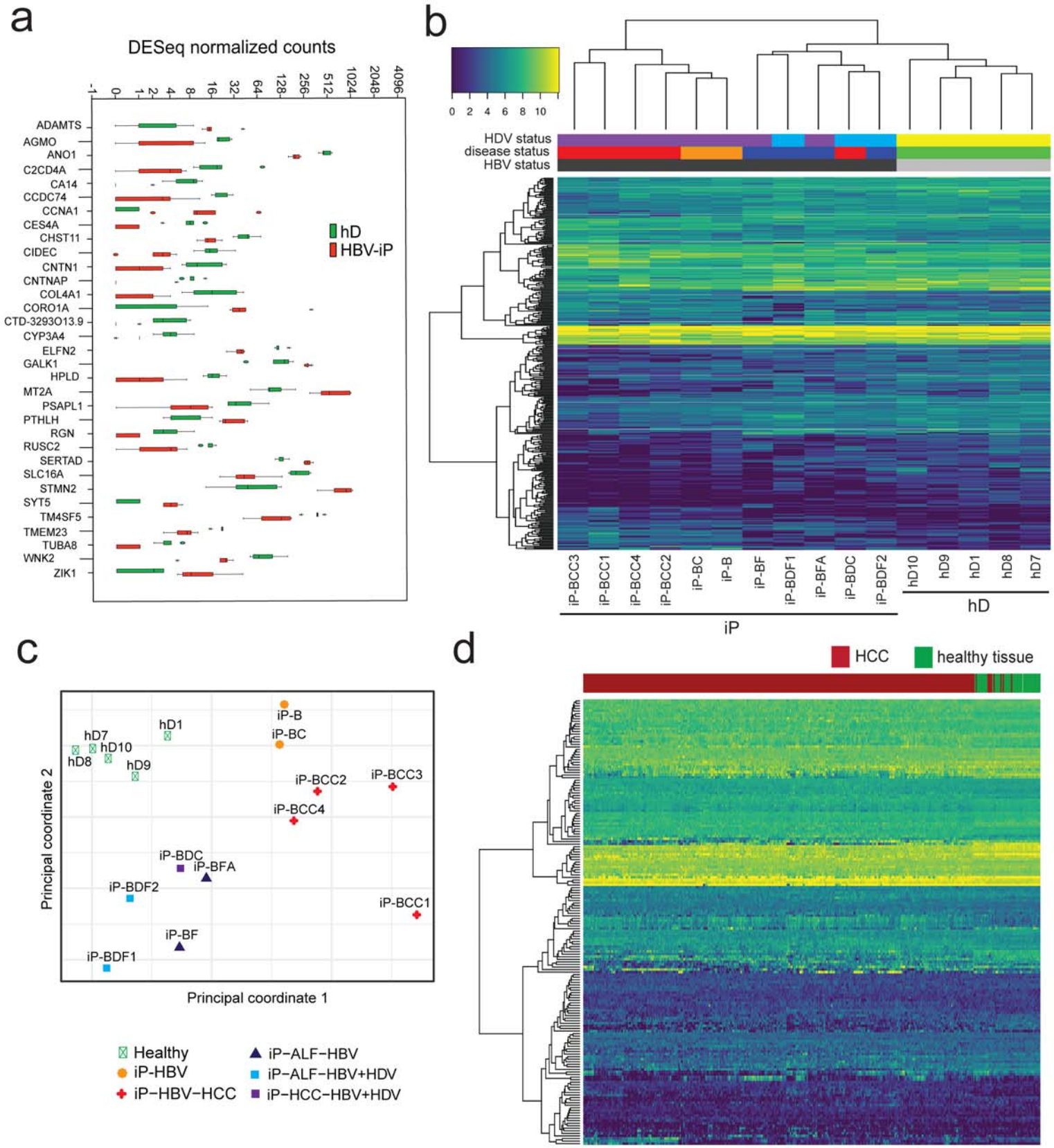

bioRxiv preprint doi: https://doi.org/10.1101/568147; this version posted March 5, 2019. The copyright holder for this preprint (which was not certified by peer review) is the author/funder. All rights reserved. No reuse allowed without permission.

Fig. 3

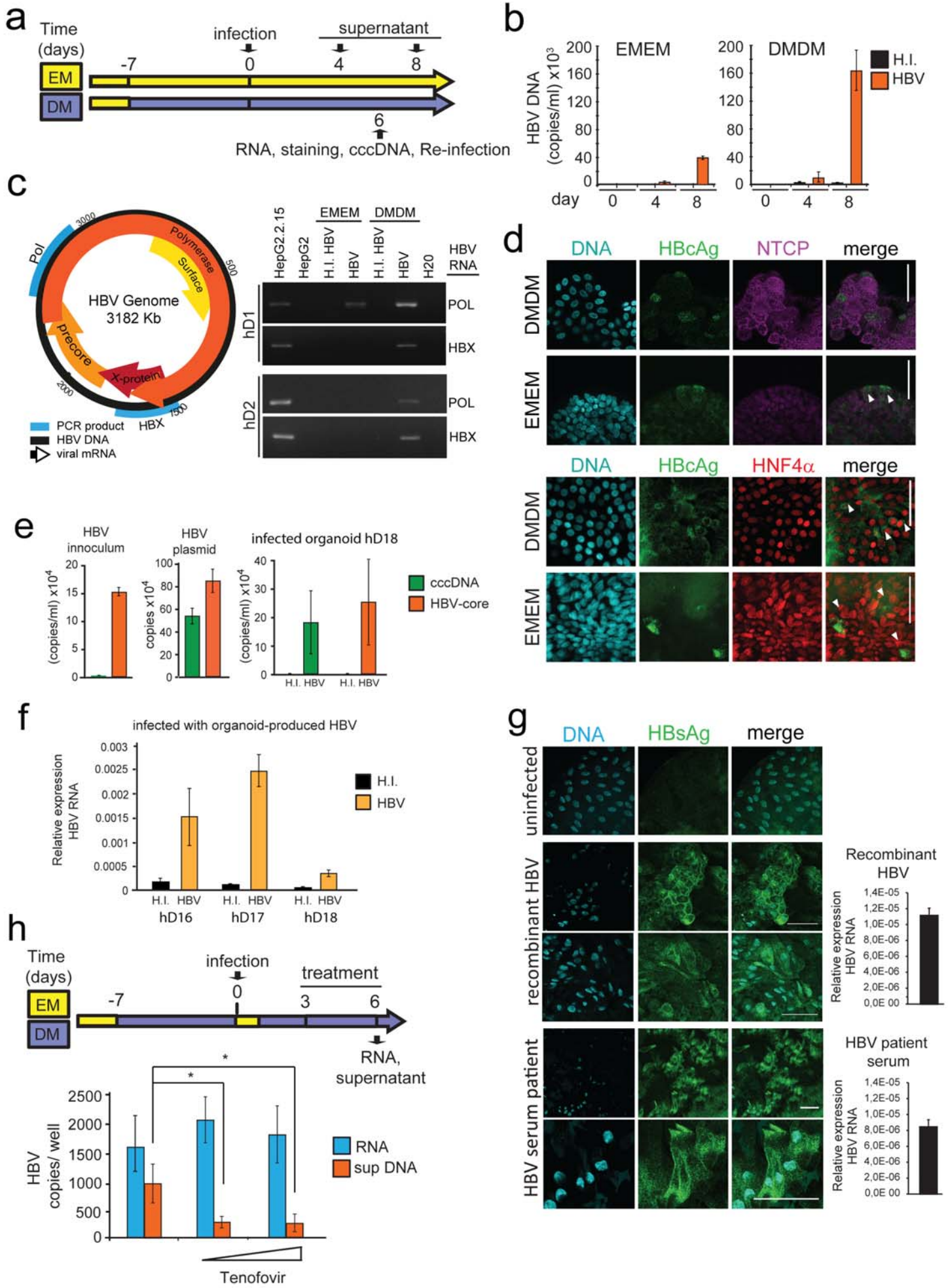

bioRxiv preprint doi: https://doi.org/10.1101/568147; this version posted March 5, 2019. The copyright holder for this preprint (which was not certified by peer review) is the author/funder. All rights reserved. No reuse allowed without permission.
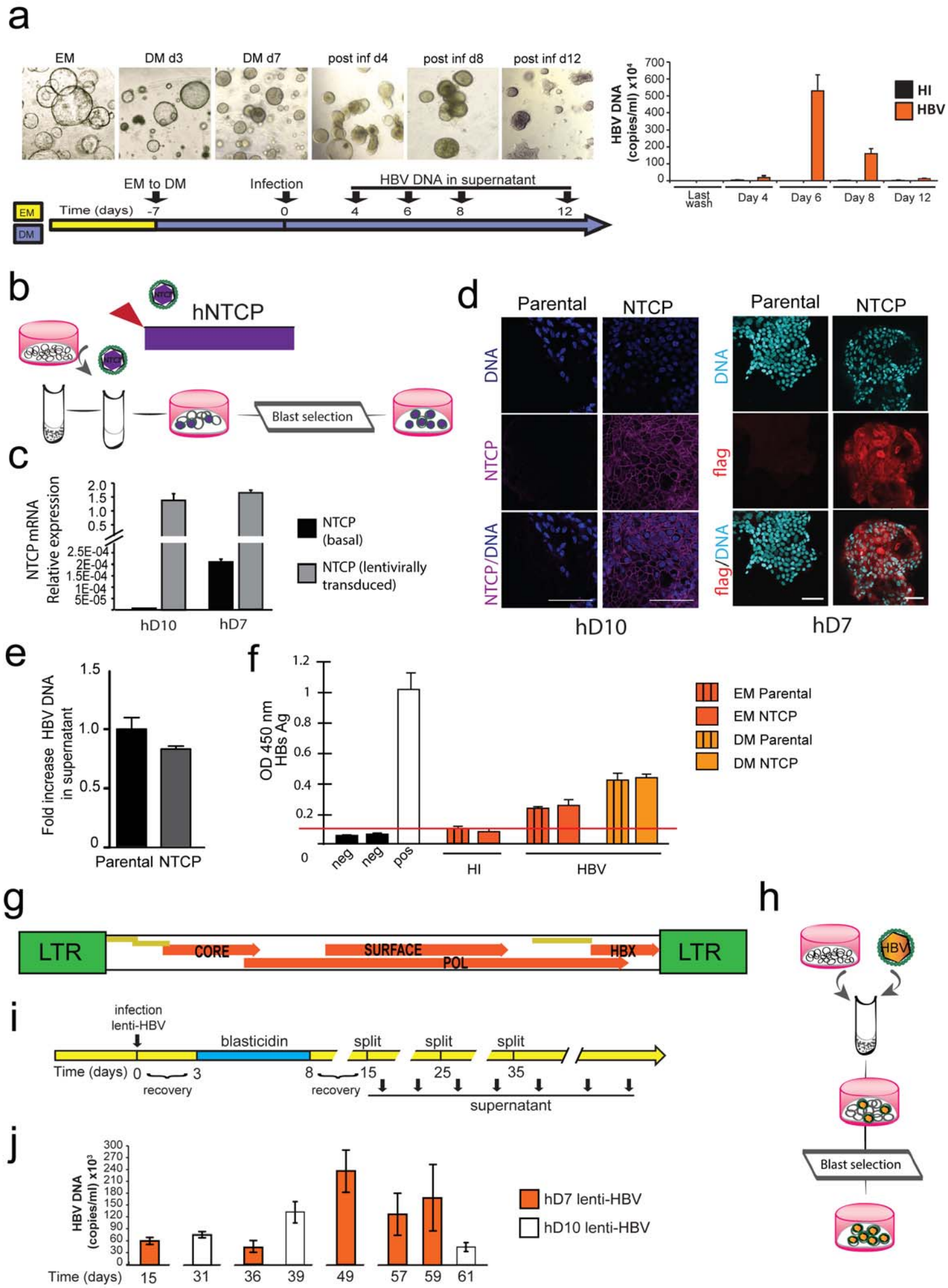
Fig. 4